Enhanced near infrared emission from the partially vitrified Nd^{3+} and silver co-doped zeolite Y

Hui Lin,[a] Sa Chu Rong Gui, Kenji Imakita, and Minoru Fujii[a]
Department of Electrical and Electronic Engineering, Graduate School of Engineering, Kobe University, Rokkodai, Nada, Kobe 657-8501, Japan

(Received 12 September 2013; accepted 2 January 2014; published online 16 January 2014)

Near infrared (NIR) emission from the Nd^{3+} doped zeolite Y was strongly enhanced by partially vitrifying the zeolite structure via extra loading silver ions and post annealing. Under the low annealing temperatures at 450 °C and 650 °C, the states of the loaded silver were determined to be the co-existence of the isolated Ag^0 atoms, the Ag^+ ions, and the Ag_2^+ dimers. However, there was no enhancement in the NIR emission by the introduction of these small silver clusters. Under higher annealing temperature at 900 °C where the lattice of the zeolite Y was partially collapsed into the amorphous phase, strong NIR emission enhancement at 1064 nm with a factor of 6.8 was observed. The partial vitrification process by the co-loading of silver and post heat-treatment had strong effect on eliminating the H_2O molecules, which can greatly enhance the NIR emission. [http://dx.doi.org/10.1063/1.4862232]

I. INTRODUCTION

Bioluminescence imaging based on the micro/nano-scale fluorescent materials has advantages like high sensitivity, low cost, high feasibility and flexibility, etc.[1–3] Previously, tremendous amount of work has been done on the visible and the near infrared (NIR) (I) (0.65–0.95 μm) "human optical window" up-conversion luminescence under the NIR excitation. Among the above, Er^{3+}, Yb^{3+} co-doped $NaYF_4$ nano-particles were most intensively investigated for the high up-conversion fluorescence quantum efficiency enabled by the low phonon energy of the $NaYF_4$ host.[4–7] Lately, a secondary "human optical window" luminescence located in the 1–1.35 μm NIR range under the NIR excitation has been explored for its promisingly low scattering from the human tissues and the low background fluorescence from the organic medicine molecules or the human tissues.[8–11] Since bioluminescence imaging often deals with the luminescence traceable drug delivery, porous materials in various forms are preferred for their strong ability of drug storage/release within the pores or the channels. Recently, self-activated porous silica nano-fibers, Er^{3+}, Yb^{3+}:$NaYF_4$ nano-crystals embedded in the porous silica nano-fibers and the porous Nd^{3+}:YAG nano-fibers have been fabricated by electrospinning and exhibited excellent bio-luminescence imaging and drug delivery properties.[12–14] Intensity variation of the up- or down-conversion emission has been observed due to the change of the environmental conditions around the luminescent enters. Speaking of the porous materials, zeolite is one of the most famous for its nature-born size, well-defined pores and channels, and actually has been put into practical use in catalysis, molecule sieving, and ion exchanging, etc. Recent research shows that zeolites are excellent luminescence host materials owing to their strong ability of separating the luminescent centers from the aggregation induced quenching.[15–18] However, due to the strong and fast non-radiative vibrational de-activation of the luminescent centers from excitation state by water molecules, or -OH bonds, reports on the NIR luminescence in the zeolite matrices were few. Tuning down the vibrational energy by extra loading the low vibrational organic guests,[19,20] or by the separation of the luminescent centers from the water molecules or the detrimental -OH bonds by partially sealing the pores with inorganic clusters[21] have been demonstrated as efficient solutions to ensure the strong NIR emission. Here, in this work, we report the enhanced NIR luminescence from partially vitrified Nd^{3+} doped zeolite Y by co-loading of silver and post heat-treatment. Nd^{3+} was chosen as the luminescent centers because the ~1.06 μm emission from the Nd^{3+}: $^4F_{3/2} \rightarrow {}^4I_{11/2}$ transition falls well in the second "human optical window" (1–1.35 μm). The Stokes shift between the Nd^{3+} 1064 nm emission and the ~800 nm NIR excitation is beneficial to accurate signal collection. Another advantage of the rare earth luminescence is that once the host matrix is determined, the emission wavelength of is fixed, independent of the excitation power or the excitation wavelength. This is favorable to the stable signal collection or even to the fingerprint identification. It also should be noted that the quantum yield of the rare earth down-conversion luminescence is usually considerably higher than that of the up-conversion process.

II. EXPERIMENTAL

A. Sample preparation

First, $Nd(NO_3)_3 \cdot 6H_2O$ was weighed and dissolved in de-ionized (DI) water to get a 50 mmol/L solution (40 mL). Then 2 g zeolite Y ($SiO_2/Al_2O_3 = 7$, Tosoh, Japan) was added into the solution and the suspension was stirred at 80 °C for 36 h. The product was centrifuged and rinsed by DI water and then dried at 80 °C. The powders were annealed from 900 °C to 1200 °C in air. Then, one half of the powders

[a]Electronic addresses: linh8112@163.com and fujii@eedept.kobe-u.ac.jp

annealed at 900 °C were stirred in a 250 mmol/L $AgNO_3$ solution (40 mL) at 80 °C for 8 h and then the aforementioned, rinsing and drying process was repeated. The dried powders were further annealed at 450 °C, 650 °C, and 900 °C in air. The obtained samples were named as $S_{Nd\text{-}\times\times\times°C\ (,\ Ag\text{-}\times\times\times°C)}$, according to the doping conditions and the annealing temperatures.

B. Characterization

The structure of the samples was investigated by X-ray diffraction (XRD) (Rigaku, Ultima IV, Japan) and FTIR (PerkinElmer, Spectrum GX, USA). Morphology of the samples was observed by transmission electron microscopy (TEM) (JSM-2100, JEOL, Japan). The valence states of the silver dopant were examined by X-ray photoelectron spectroscopy (XPS) (Automated XPS Microprobe PHI X-tool-ULVAC-PHI, Japan). Diffuse reflection spectra of the samples were measured by a UV/VIS/NIR spectrometer (Shimazu 3700, Japan). Photoluminescence (PL) and photoluminescence excitation (PLE) spectra were measured on a spectrofluorometer (Horiba Fluorog 3 Jovin, Japan). The decay time of the Nd^{3+} 1064 nm emission under the 803 nm excitation from an optical parametric oscillator (OPO) pumped by a third harmonic Nd:YAG laser was measured by a photomultiplier tube (Hamamatsu, R5509-72), and then the signal was analyzed with a photon-counting multichannel scaler. For all the optical spectra measurement, the samples were loosely packed into the sample holder without any solvent.

III. RESULTS AND DISCUSSION

XRD θ-2θ scans of the Nd^{3+} doped zeolites with different annealing temperatures are presented in Fig. 1(a). The diffraction patterns for the samples annealed at 900 °C are identical to zeolite Y (JCPDS43-0168), which indicated that the zeolite structure was not changed. However, the diffraction intensity became weaker for $S_{Nd\text{-}900\,°C}$ compared with that of the untreated pure zeolite Y. Annealing at 950 °C may be a critical point since the zeolite diffraction intensity became further weaker and a broad amorphous band began to turn out. For the samples annealed at 1000 °C, the composition of the sample was separated into mullite $Al_6Si_2O_{13}$ (JCPDS15-0776) and amorphous phase. When annealed at 1100 °C, a new phase, cristobalite silica (JCPDS39-1425) turned out, coexisting with the mullite $Al_6Si_2O_{13}$ and the amorphous phase. When annealed at 1200 °C, the amorphous phase almost fully turned into the cristobalite phase silica and the sample was of SiO_2 and $Al_6Si_2O_{13}$ mixed phases.

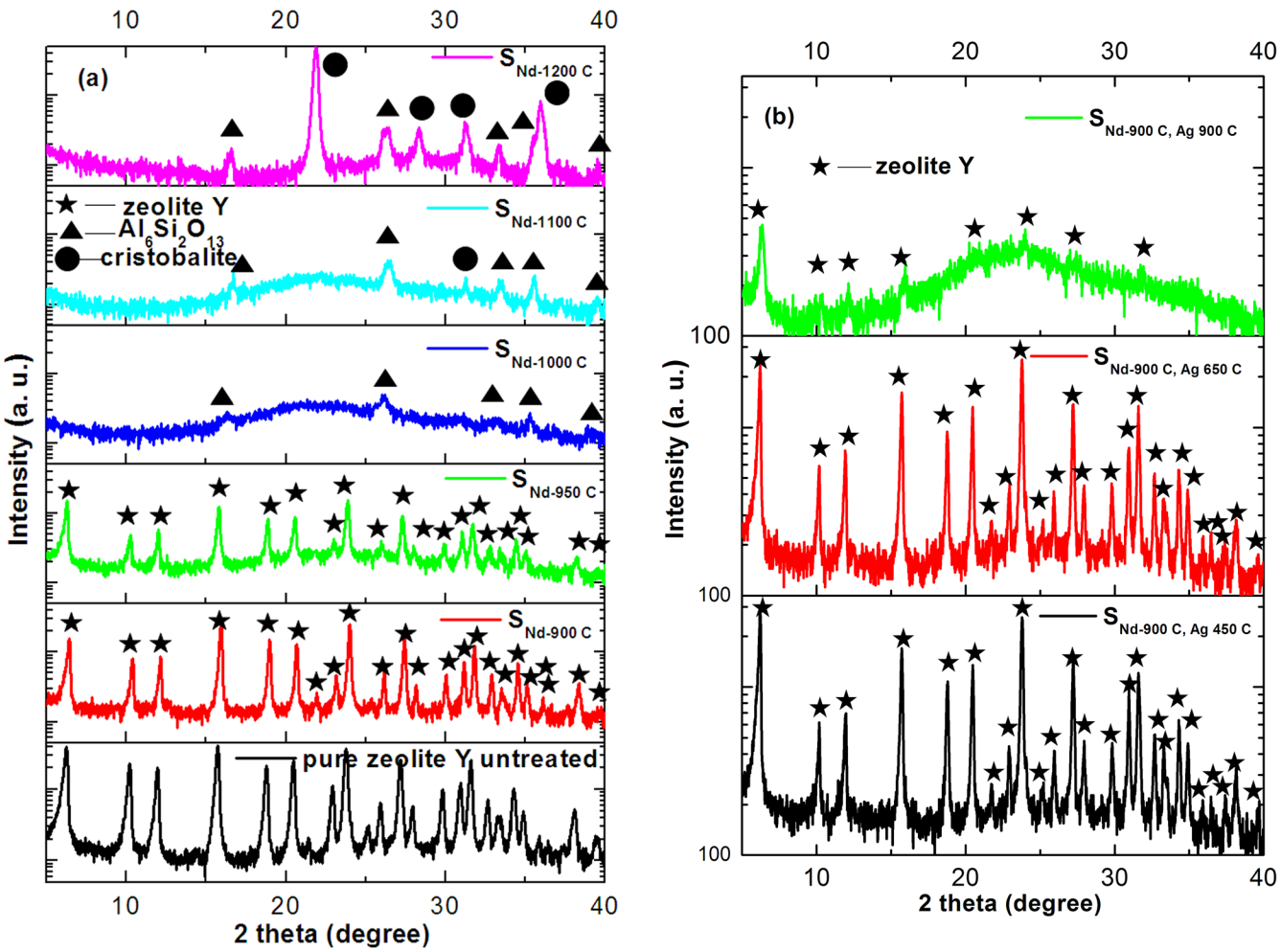

FIG. 1. XRD θ-2θ scans of the Nd^{3+} single doped (a) and the Nd^{3+}, silver co-doped (b) zeolites under different annealing temperatures; the diffraction peaks were indentified: ★ for zeolite Y, ▲ for $Al_6Si_2O_{13}$, and ● for cristobalite phase silica.

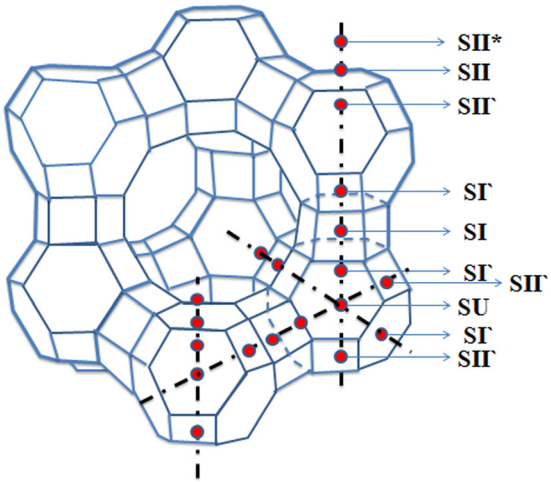

FIG. 2. Schematic diagrams showing the cation sites in the ideal zeolite Y framework: the blue skeleton stands for the zeolite Y framework, and the red balls stand for the cation sites.

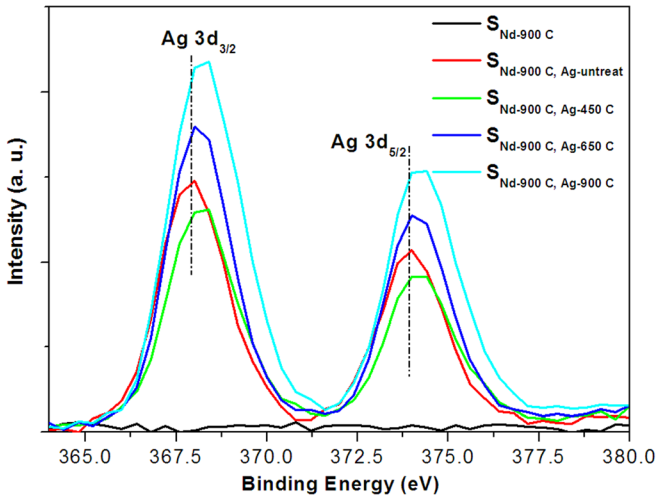

FIG. 3. XPS spectra for the Nd^{3+} and silver doped zeolite Y samples.

XRD θ–2θ scans of the Nd^{3+} and silver co-loaded zeolite Y are given in Fig. 1(b). It can be seen that compared with the untreated pure zeolite Y, the diffraction intensity was decreased for $S_{Nd\text{-}900\,^\circ C,\ Ag\text{-}450\,^\circ C}$, and $S_{Nd\text{-}900\,^\circ C,\ Ag\text{-}650\,^\circ C}$. While for $S_{Nd\text{-}900\,^\circ C,\ Ag\text{-}900\,^\circ C}$, the diffraction intensity from zeolite Y became very weak and a characteristic amorphous broad band turned up. It is interesting that unlike $S_{Nd\text{-}1000\,^\circ C}$ and $S_{Nd\text{-}1100\,^\circ C}$ for which the zeolite Y phase was totally sacrificed and the new phase (mullite) turned up instead, while the zeolite Y structure was still partially maintained for $S_{Nd\text{-}900\,^\circ C,\ Ag\text{-}900\,^\circ C}$ without showing extra crystalline phases.

Schematic diagram of the ideal zeolite Y structure is presented in Fig. 2. There are a set of well defined sites for the cations in the zeolite Y structure.[22] SI is located in the center of the hexagonal prism which is inaccessible to the detrimental -OH bonds or the water molecules. SI′ is located in sodalite cage close to the center of the prism-sodalite shared 6-member ring. Ag_2^+ dimers can be formed with one Ag^0 atom occupying the SI site linked to one Ag^+ occupying the SI′ site.[23] SII′ is located in the sodalite cage close to the center of the sodalite self-own 6-member ring. SII is in the super cage, next to SII′ and in line with SII and the center of the sodalite self-own 6-ring. Recent study based on PL spectra and high-resolution powder XRD shows that NIR luminescent centers such as Bi^+ located in the sodalite cage mainly contribute to emission.[24] SII* is located deeper in the super cage and also in line with SII′ and SII. SU is in the center of the sodalite cage. Thus, the luminescent centers located at the SI′, SII′, SII, S II*, and SU sites in the sodalite cage and the super cage are vulnerable to be quenched by the existence or the entrance of the water molecules or the highly vibrational -OH bonds.

XPS spectra of silver for all the silver doped samples and $S_{Nd\text{-}900\,^\circ C}$ were shown in Fig. 3. Except for $S_{Nd\text{-}900\,^\circ C}$, the two peaks for Ag $3d_{3/2}$ and Ag $3d_{5/2}$ located at 368.3 eV and 374.3 eV were detected for all the silver doped samples with post heat-treatment. There was a 0.3 eV negative shift each for the Ag $3d_{3/2}$ and the Ag $3d_{5/2}$ peaks, compared with the counterparts of $S_{Nd\text{-}900\,^\circ C,\ Ag\text{-}untreat}$ (Ag $3d_{3/2}$ @ 368.0 eV and Ag $3d_{5/2}$ @ 374.0 eV, respectively). The negative shifts indicated the partial reduction of Ag^+ ions into Ag^0 atoms

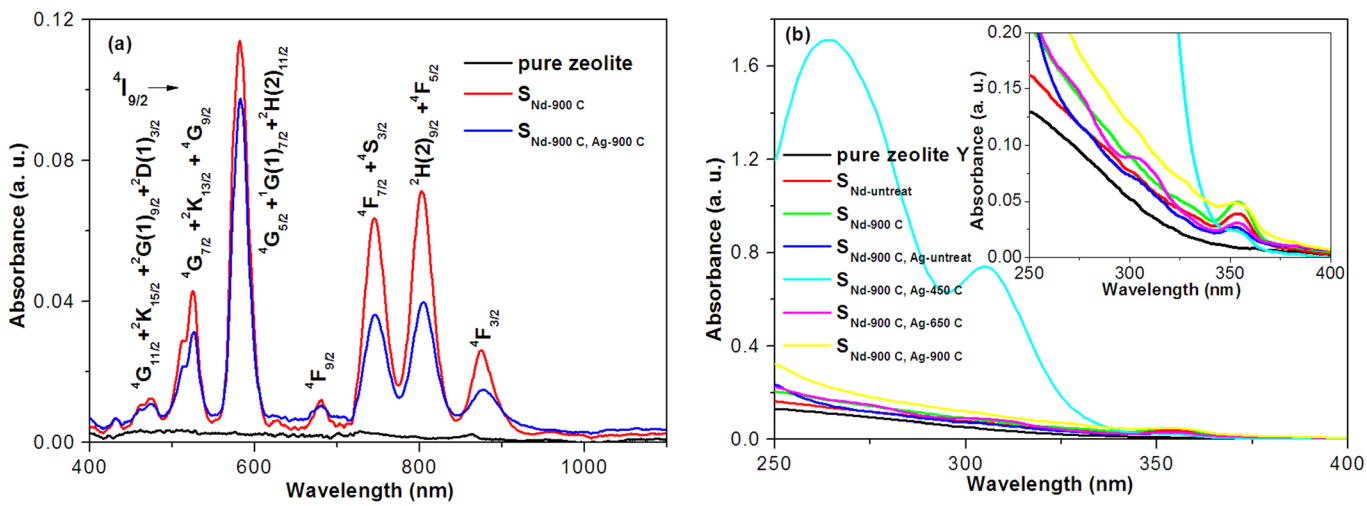

FIG. 4. Absorption spectra of the samples derived from the Kubelka-Monk formula in the visible-NIR range (a) and the UV range (b); the inset in Fig. 3(b) is a magnified view.

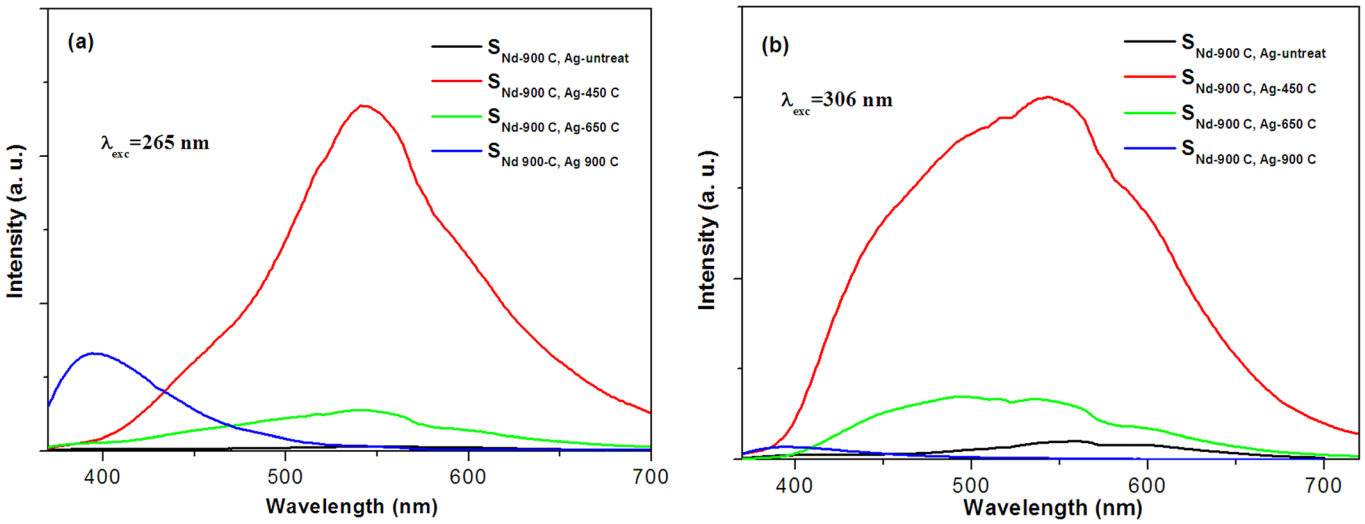

FIG. 5. PL spectra of $S_{Nd\text{-}900\,^{\circ}C,\ Ag\text{-}untreat}$, $S_{Nd\text{-}900\,^{\circ}C,\ Ag\text{-}450\,^{\circ}C}$, $S_{Nd\text{-}900\,^{\circ}C,\ Ag\text{-}650\,^{\circ}C}$, and $S_{Nd\text{-}900\,^{\circ}C,\ Ag\text{-}900\,^{\circ}C}$ under the 265 nm (a) and the 306 nm (b) excitations in the visible range.

during the post heat-treatment process.[25] The formation of Ag^0 atom from Ag^+ ion can be through the negative charge transfer from the framework O^{2-} or water as the reducing agent.[26] However, it is not suitable to estimate the ratio of Ag^0/Ag^+, since it is difficult to distinguish Ag^0 atoms from Ag^+ ions in the XPS spectra accurately for quantitative calculation.

The absorption peaks due to the transitions from the Nd^{3+}: $^4I_{9/2}$ ground state to the higher energy states have been assigned in Fig. 4(a). Due to the Nd^{3+}-Ag^+ ion exchanging during the loading of the Ag^+, the absorption of Nd^{3+} became lower than that of the Nd^{3+} single doped samples. The absorption spectra in the UV range were presented in Fig. 4(b). For $S_{Nd\text{-}900\,^{\circ}C,\ Ag\text{-}untreat}$, the absorption of silver was almost negligible. For $S_{Nd\text{-}900\,^{\circ}C,\ Ag\text{-}450\,^{\circ}C}$ and $S_{Nd\text{-}900\,^{\circ}C,\ Ag\text{-}650\,^{\circ}C}$, the absorption peak located at 265 nm is assigned to the Ag^+ ions.[27] The absorption at 306 nm for $S_{Nd\text{-}900\,^{\circ}C,\ Ag\text{-}450\,^{\circ}C}$ and $S_{Nd\text{-}900\,^{\circ}C,\ Ag\text{-}650\,^{\circ}C}$ was attributed to the 2S→2P transition of the isolated Ag^0 atom located in the center of the hexagonal prism.[23,28] For $S_{Nd\text{-}900\,^{\circ}C,\ Ag\text{-}900\,^{\circ}C}$, the 265 nm and the 306 nm absorption peaks totally disappeared, and no other new absorption peaks were detected.

To further determine the states of the loaded silver, the emission spectra in the visible range under the 265 nm and the 306 nm excitation were investigated. For $S_{Nd\text{-}900\,^{\circ}C,\ Ag\text{-}450\,^{\circ}C}$ and $S_{Nd\text{-}900\,^{\circ}C,\ Ag\text{-}650\,^{\circ}C}$, the strongest emission peaks under the 265 nm excitation was both located at 544 nm (see Fig. 5), which was attributed to Ag^0 atoms from the Ag^0(SI)-Ag^+(SI′) dimers.[25] While for $S_{Nd\text{-}900\,^{\circ}C,\ Ag\text{-}900\,^{\circ}C}$ under the 265 nm excitation, a new emission peak centered at 394 nm turned up. This emission band may be attributed to the oxygen vacancy defects, since for the untreated pure zeolite Y, a similar emission band with a lower intensity has also been observed. Under the 306 nm excitation, two strong emission peaks located at 494 nm and 544 nm were observed for $S_{Nd\text{-}900\,^{\circ}C,\ Ag\text{-}450\,^{\circ}C}$ and $S_{Nd\text{-}900\,^{\circ}C,\ Ag\text{-}650\,^{\circ}C}$. The 494 nm emission was attributed to the emission from the isolated Ag^0 atom at site SI in the hexagonal prism.[29] One clear tendency that can be seen is that the intensity of these emissions dropped drastically when annealed at 650 °C and 900 °C,

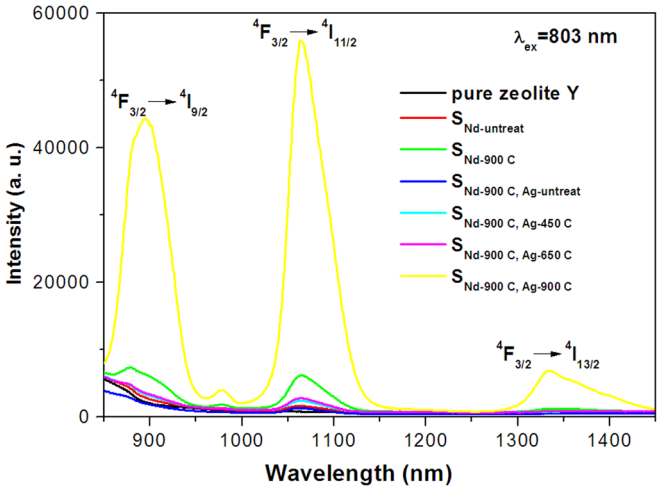

FIG. 6. NIR emission spectra of the Nd^{3+} (and silver) doped zeolite Y samples.

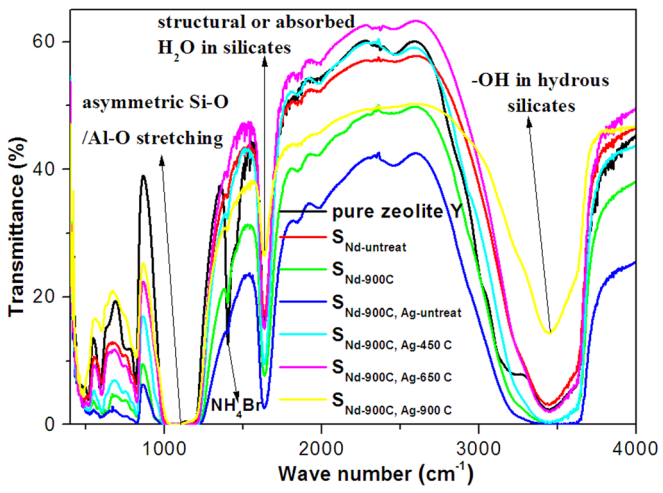

FIG. 7. FTIR spectra for the pure zeolite Y, $S_{Nd\text{-}untreat}$, $S_{Nd\text{-}900\,^{\circ}C}$, $S_{Nd\text{-}900\,^{\circ}C,\ Ag\text{-}untreat}$, $S_{Nd\text{-}900\,^{\circ}C,\ Ag\text{-}450\,^{\circ}C}$, $S_{Nd\text{-}900\,^{\circ}C,\ Ag\text{-}650\,^{\circ}C}$, and $S_{Nd\text{-}900\,^{\circ}C,\ Ag\text{-}900\,^{\circ}C}$.

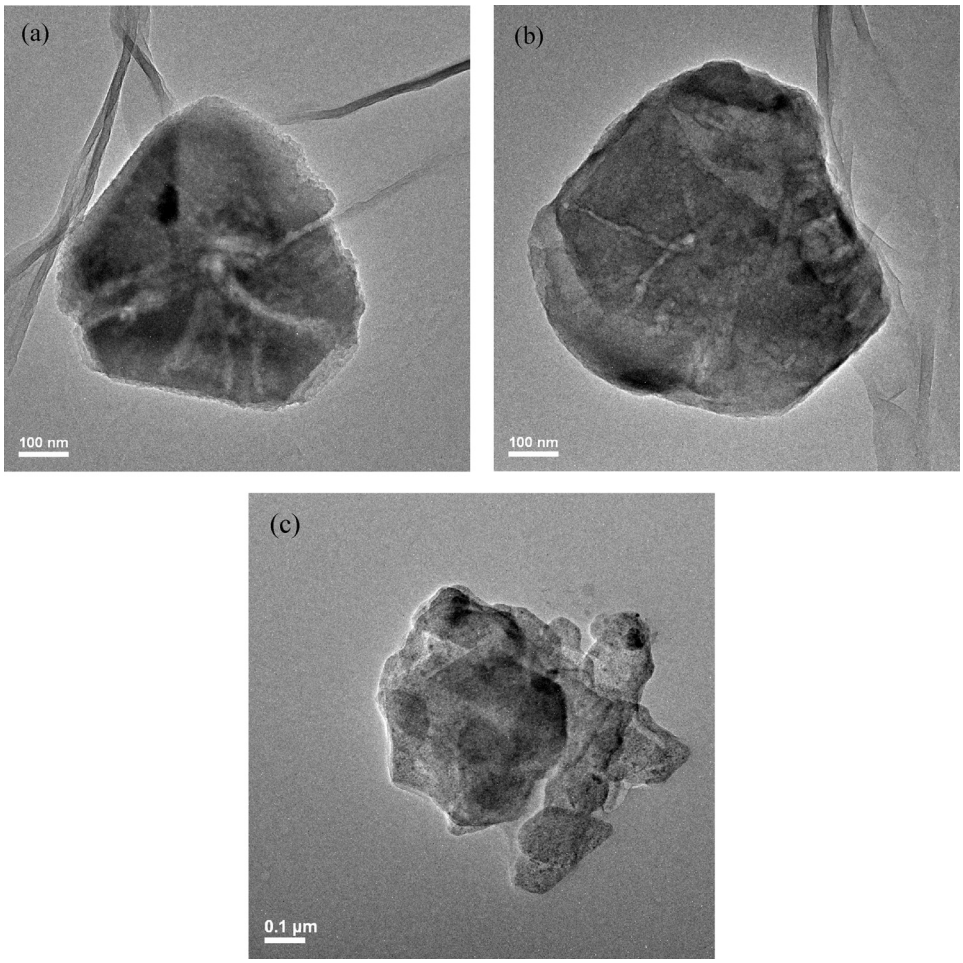

FIG. 8. TEM morphology of pure zeolite Y (a), $S_{Nd\text{-}900\,^{\circ}C}$ (b), and $S_{Nd\text{-}900\,^{\circ}C,\ Ag\text{-}900\,^{\circ}C}$ (c) individual particles.

which was in accordance with the absorption spectra and implied that the small silver clusters may turn into large particles or may be incorporated into the amorphous phase at high heat-treatment temperatures. For $S_{Nd\text{-}900\,^{\circ}C,\ Ag\text{-}900\,^{\circ}C}$, there was no emission in the visible range under the 306 nm excitation. The shapes of the emission peaks under the 265 nm and 306 nm excitations for $S_{Nd\text{-}900\,^{\circ}C,\ Ag\text{-}untreat}$ were similar to the counterparts of $S_{Nd\text{-}900\,^{\circ}C,\ Ag\text{-}450\,^{\circ}C}$. However, the emission intensity decreased by ~1 order of magnitude.

Seen from the PL spectra in the NIR range (shown in Fig. 6), there was no emission in the NIR range upon the 803 nm excitation for the untreated pure zeolite Y. The NIR emission for the sample without annealing was the weakest among the Nd^{3+} doped samples. For $S_{Nd\text{-}900\,^{\circ}C,\ Ag\text{-}450\,^{\circ}C}$ and $S_{Nd\text{-}900\,^{\circ}C,\ Ag\text{-}650\,^{\circ}C}$, the integrated emission intensity for the 1064 nm emission both dropped about 42.4%, compared with that of $S_{Nd\text{-}900\,^{\circ}C}$. The possible reason is that these samples got hydrated again to some extent during the silver loading and the second round low temperature thermal treatment at 450 °C and 650 °C. In addition, Ag^{+} ions, Ag^{0} atoms and Ag^{0}(SI)-Ag^{+}(SI′) dimers were too small to isolate the Nd^{3+} luminescent centers from the -OH bonds and the H_2O molecules, thus made no positive contribution to the NIR emission of Nd^{3+}. For $S_{Nd\text{-}900\,^{\circ}C,\ Ag\text{-}900\,^{\circ}C}$, there was a large enhancement with a factor of 6.8 for the integrated 1064 nm emission compared with the counterpart of $S_{Nd\text{-}900\,^{\circ}C}$. Since there was no absorption around 803 nm from silver in the absorption spectra, the enhanced NIR emission cannot be attributed to the energy transfer from silver to Nd^{3+}. It was reasonable that the partially vitrification by annealing the silver co-loaded sample at 900 °C made the main contribution to the NIR emission enhancement. In this case, the role of the low vibrational organic compounds (bis(perfluoromethylsulfonyl)amine, PMS-H) in the zeolite framework was so obvious that strong

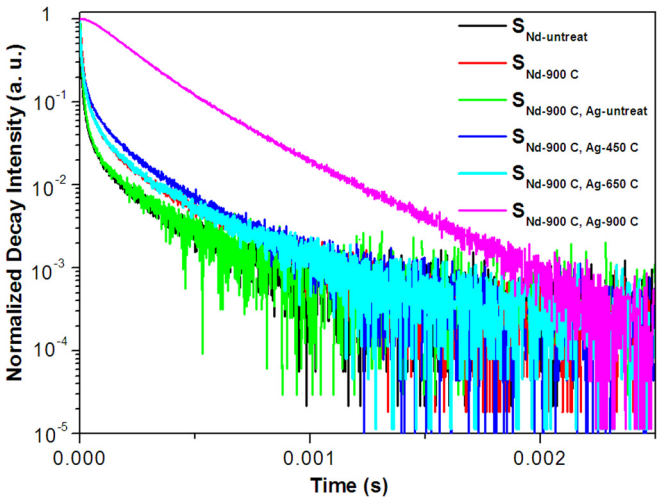

FIG. 9. Decay curves for the Nd^{3+} 1064 nm emission under the 803 nm excitation.

TABLE I. Decay time of the Nd^{3+} 1064 nm emission under the 803 nm excitation.

Sample name	$S_{Nd\text{-}untreat}$	$S_{Nd\text{-}900\,^{\circ}C}$	$S_{Nd\text{-}900\,^{\circ}C,Ag\text{-}untreat}$	$S_{Nd\text{-}900\,^{\circ}C,Ag\text{-}450\,^{\circ}C}$	$S_{Nd\text{-}900\,^{\circ}C,Ag\text{-}650\,^{\circ}C}$	$S_{Nd\text{-}900\,^{\circ}C,\,Ag\text{-}900\,^{\circ}C}$
Decay time (μs)	11	23	13	25	21	237

NIR emission could be observed even for the sample directly dried at 150 °C without high temperature annealing, which may be attributed to the strong combination between the PMS-H and the -OH bonds.[19]

FTIR spectra were measured to take a further look at the microstructure evaluation of the zeolite, as shown in Fig. 7. The characteristic absorption bands of the -OH bonds located around 3400 cm^{-1} to 3600 cm^{-1} were observed in the FTIR spectra.[22] For $S_{Nd\text{-}900\,^{\circ}C,\,Ag\text{-}450\,^{\circ}C}$ and $S_{Nd\text{-}900\,^{\circ}C,\,Ag\text{-}650\,^{\circ}C}$, the amount of the -OH bonds did not seem to be reduced at all. For $S_{Nd\text{-}900\,^{\circ}C,\,Ag\text{-}900\,^{\circ}C}$, the -OH absorption band became slightly lower, which implied that at 900 °C silver had positive effect on eliminating the high vibrational -OH bonds by vitrifying the zeolite Y structure during the postannealing dehydration process. The absorption band located at 1634 cm^{-1} is attributed to the structural or absorbed H_2O in the silicates.[30] For $S_{Nd\text{-}900\,^{\circ}C,\,Ag\text{-}900\,^{\circ}C}$, the absorption at 1634 cm^{-1} was reduced at least 50% compared with other samples. This was believed to be the main reason for the strong enhancement for the NIR emission. For the pure zeolite Y, the sharp absorption peak located at 1400 cm^{-1} is attributed to NH_4Br. Since the other samples were ion-exchanged with Nd^{3+} and Ag^{+}, the absorption by NH_4Br in the FTIR spectra has been greatly reduced. The intense absorption band around 1100 cm^{-1} was the characteristic asymmetric Si-O/Al-O stretching vibration.[16]

TEM morphology of pure zeolite Y clearly exhibits the typical polyhedron profile (Fig. 8(a)). The morphology of $S_{Nd\text{-}900\,^{\circ}C}$ shown in Fig. 8(b) is similar to that of pure zeolite Y. While for $S_{Nd\text{-}900\,^{\circ}C,\,Ag\text{-}900\,^{\circ}C}$, collapse of the polyhedron morphology can be clearly observed in Fig. 8(c). Large silver nano-particles were not observed for $S_{Nd\text{-}900\,^{\circ}C,\,Ag\text{-}900\,^{\circ}C}$, which may be attributed to the low doping concentration of silver in the zeolite Y framework. Based on the semi-quantitative calculation from the XPS data, the atomic concentration of silver is ~1%. Small silver cluster like Ag_2^{+} dimer whose scale is less than 1 nm, is insensitive to TEM or XRD θ-2θ detection but sensitive to optical spectra.

The decay curves of the Nd^{3+} 1064 nm emission were given in Fig. 9. The decay curves of the Nd^{3+} 1064 nm emission for $S_{Nd\text{-}untreat}$, $S_{Nd\text{-}900\,^{\circ}C}$, $S_{Nd\text{-}900\,^{\circ}C,\,Ag\text{-}untreat}$, $SS_{Nd\text{-}900\,^{\circ}C,\,Ag\text{-}450\,^{\circ}C}$ and $S_{Nd\text{-}900\,^{\circ}C,\,Ag\text{-}650\,^{\circ}C}$ all showed at least two exponential decay features. The mean decay time (τ_m) values calculated from the equation $\tau_m = \int_{t_0}^{\infty}[I(t)/I_0]dt$, (where $I(t)$ is luminescence decay Intensity at time t, I_0 is the maximal value of the decay intensity, and t_0 corresponds to the initial time when I_0 occurs), as listed in Table I, were close to the data (22 μs) reported in Ref. 19. The slight drop in the emission lifetime for $S_{Nd\text{-}900\,^{\circ}C,\,Ag\text{-}650\,^{\circ}C}$ implied that the structure collapse of the crystalline zeolite Y might start. While for $S_{Nd\text{-}900\,^{\circ}C,\,Ag\text{-}900\,^{\circ}C}$, the emission decay time rocketed to 237 μs, which was close to that of the Nd:YAG single crystal (254 μs for the 0.1 at. % Nd:YAG).[31] The strong NIR emission in the NIR (II) range, the large Stokes shift, and the long emission decay time together make the Nd^{3+} doped zeolite Y with silver as a dehydration catalyst a very promising material for the luminescence traceable drug delivery. For practical bio-application, water solubility is a key issue to be solved, so surface modifications, like ligands exchange,[32] for instance, will be conducted in order to achieve a hydrophilic surface in our future work.

IV. CONCLUSIONS

The 1064 nm NIR emission from the Nd^{3+} doped zeolite Y has been enhanced by partially collapsing the porous zeolite structure into the amorphous phase with the co-loading of silver and the post heat-treatment. The emission decay time at 1064 nm under the 803 nm excitation reached 237 μs, which was close to that of the Nd:YAG laser crystals. The reason for the enhanced emission intensity and the prolonged emission decay time is mainly due to the promoted elimination of the H_2O molecules from the zeolite Y from framework. The strong NIR emission from the Nd^{3+} doped zeolite materials may have applications for the luminescence traceable drug delivery.

[1]B. J. Tromberg, N. Shah, R. Lanning, A. Cerussi, J. Espinoza, T. Pham, L. Svaasand, and J. Butler, Neoplasia **2**(1–2), 26–40 (2000).
[2]F. Pinaud, X. Michalet, L. A. Bentolila, J. M. Tsay, S. Doosel, J. J. Li, G. Iyer, and S. Weiss, Biomaterials **27**(9), 1679–1687 (2006).
[3]M.-K. So, C. Xu, A. M. Loening, S. S. Gambhir, and J. Rao, Nat. Biotechnol. **24**(3), 339–343 (2006).
[4]J. H. Zeng, J. Su, Z. H. Li, R. X. Yan, and Y. D. Li, Adv. Mater. **17**, 2119–2123 (2005).
[5]M. Fujii, T. Nakano, K. Imakita, and S. Hayashi, J. Phys. Chem. C **117**, 1113–1120 (2013).
[6]S. Heer, K. Kömpe, H.-U. Güdel, and M. Haase, Adv. Mater. **16**, 2102–2105 (2004).
[7]D. K. Chatterjee, A. J. Rufaihah, and Y. Zhang, Biomaterials **29**, 937–943 (2008).
[8]G. Hong, J. C. Lee, J. T. Robinson, U. Raaz, L. Xie, N. F. Huang, J. P. Cooke, and H. Dai, Nat. Med. **18**(12), 1841–1848 (2012).
[9]Y. Zhang, Y. Zhang, G. Hong, W. He, K. Zhou, K. Yang, F. Li, G. Chen, Z. Liu, H. Dai, and Q. Wang, Biomaterials **34**, 3639–3646 (2013).
[10]Y. Zhang, G. Hong, Y. Zhang, G. Chen, F. Li, H. Dai, and Q. Wang, ACS Nano **6**(5), 3695–3702 (2012).
[11]A. M. Smith, M. C. Mancini, and S. Nie, Nat. Nanotechnol. **4**(11), 710–711 (2009).
[12]Z. Hou, C. Zhang, C. Li, Z. Xu, Z. Cheng, G. Li, W. Wang, C. Peng, and J. Lin, Chem. Eur. J. **16**, 14513–14519 (2010).
[13]Z. Hou, C. Li, P. Ma, G. Li, Z. Cheng, C. Peng, D. Yang, P. Yang, and J. Lin, Adv. Funct. Mater. **21**, 2356–2365 (2011).
[14]Z. Ma, H. Ji, D. Tan, G. Dong, Y. Teng, J. Zhou, and J. Qiu, Chem. Eur. J. **18**, 2609–2616 (2012).
[15]Y. Wada, M. Sato, and Y. Tsukahara, Angew. Chem. Int. Ed. **45**, 1925–1928 (2006).
[16]H. Li, H. Zhang, L. Wang, D. Mu, S. Qi, X. Hu, L. Zhang, and J. Yuan, J. Mater. Chem. **22**, 9338–9342 (2012).
[17]A. Z. Ruiz, H. Li, and G. Calzaferri, Angew. Chem. Int. Ed. **45**, 5282–5287 (2006).
[18]W. Chen, R. Sammynaiken, and Y. Huang, J. Appl. Phys. **88**(3), 1424–1431 (2000).

[19]Y. Wada, T. Okubo, M. Ryo, T. Nakazawa, Y. Hasegawa, and S. Yanagida, J. Am. Chem. Soc. **122**, 8583–8584 (2000).
[20]M. Ryo, Y. Wada, T. Okubo, Y. Hasegawa, and S. Yanagida, J. Phys. Chem. B **107**, 11302–11306 (2003).
[21]H. T. Sun, A. Hosokawa, Y. Miwa, F. Shimaoka, M. Fujii, M. Mizuhata, S. Hayashi, and S. Deki, Adv. Mater. **21**, 3694–3698 (2009).
[22]J. V. Smith, Adv. Chem. Ser. **101**, 171 (1974).
[23]G. A. Ozin and F. Hugues, J. Phys. Chem **87**, 94–97 (1983).
[24]H.-T. Sun, Y. Matsushita, Y. Sakka, N. Shirahata, M. Tanaka, Y. Katsuya, H. Gao, and K. Kobayashi, J. Am. Chem. Soc. **134**, 2918–2921 (2012).
[25]N. D. Hutson, B. A. Reisner, R. T. Yang, and B. H. Toby, Chem. Mater. **12**, 3020–3031 (2000).
[26]H.-T. Sun, Y. Sakka, N. Shirahata, Y. Matsushita, K. Deguchi, and T. Shimizu, J. Phys. Chem. C **117**, 6399–6408 (2013).
[27]L. R. Gellens and R. A. Schoonheydt, in *Metal Microstructures in Zeolites*, edited by P. A. Jacobs, N. I. Jaeger, P. Jira, and G. Schult-Ekloff (Elsevier, Amsterdam, 1982), p. 87.
[28]D. R. Brown and L. Kevan, J. Phys. Chem. **90**, 1129–1133 (1986).
[29]R. Kellerman and J. Texter, J. Chem. Phys. **70**, 1562 (1979).
[30]Y. Kebukawa, C. M. O'D. Alexander, and G. D. Cody, in *Proceedings of the 76th Annual Meteoritical Society Meeting* (2013), p. 5091.
[31]H. Yagi, T. Yanagitani, K. Takaichi, K. Ueda b, and A. A. Kaminskii, Opt. Mater. **29**, 1258–1262 (2007).
[32]W. C. W. Chan and S. Nie, Science **281**, 2016–2018 (1998).